Research Article

Advances in Mechanical Engineering

Advances in Mechanical Engineering
2024, Vol. 16(6) 1–16
© The Author(s) 2024
DOI: 10.1177/16878132241263940
journals.sagepub.com/home/ade
Sage

Optimization of dynamic parameter design of Stewart platform with Particle Swarm Optimization (PSO) algorithm

Masood Shahbazi[1], Mohammadreza Heidari[2] and Milad Ahmadzadeh[3]

Abstract

Today motion simulators are being produced rely on electric actuators. The conventional way of dealing with high velocity, accelerations, and bulky payload is using a bigger actuator, but this leads to increased power usage and costs. To overcome these limitations, an optimized design of the Stewart platform design parameter improves simulators' ability to support the weight of the equipment and satisfy the desired velocity and acceleration. However, it is challenging to set platform design parameters to maintain efficiency across the entire workspace. In this article, the kinematics and dynamics of the six-axis general Stewart robot are explored. A high-rated desired velocity and acceleration for the Stewart platform are defined and simulated. Then, the electric actuator force during some motion trajectory based on the defined workspace, velocity, and acceleration are calculated. Particle Swarm Optimization (PSO) is employed to optimize platform design parameters. The algorithm defines a cost function to minimize the maximum speed and maximum Force of the actuator by examining the structural kinematics arrangement of design parameters. Findings demonstrate that optimized design parameters have been successful in reducing the maximum actuator power 88.3%. Additionally, improves Stewart platform mechanical components' life. These procedures can be employed for any Stewart platform.

Keywords

Particle Swarm Optimization (PSO) algorithm, parallel manipulators, Stewart platform, motion simulator, electric actuators, actuator power

Date received: 9 December 2023; accepted: 3 June 2024

Handling Editor: Sharmili Pandian

Introduction

The advent of parallel robots marked a significant breakthrough in the area of robotics, ushering in a multitude of challenges for roboticists. While parallel manipulators offer advantages more than serial manipulators such as structurally rigidity, accuracy in positioning, low inertia, high stiffness, and substantial payload capacity, they also face challenges such as limited workspace and singularity.[1–5] Calculating the parallel manipulator workspace is a more intricate task compared to a serial link manipulator, as the translation capabilities of the

[1]Department of Mechanical Engineering, Razi University, Kermanshah, Iran
[2]Department of Mechanical Engineering, Kermanshah University of Technology, Kermanshah, Iran
[3]Department of Electrical Engineering, Amirkabir University of Technology (Tehran Polytechnic), Tehran, Iran

Corresponding author:
Masood Shahbazi, Department of Mechanical Engineering, Razi University, Taq-e Bostan, Kermanshah 6714414971, Iran.
Email: masoodshahbaz90@gmail.com

former are contingent upon the orientation of the end-effector.[6] The determination of the workspace is a crucial aspect of the design process for parallel manipulators. In the case of 6-degree-of-freedom (DOF) parallel manipulators, the limitations of their workspace are influenced by factors such as the limit of linear actuators, mechanical constraints on passive joints, and interferences between links.[6] Unlike serial manipulators with openloop architectures, parallel manipulators are characterized by closed-loop kinematic structures.[7]

The concept of parallel mechanical architectures was presented firstly for testing tire by Gough and then adopted by Stewart for motion simulators, capitalizing on their unbeatable advantages compared to serial mechanisms.[8,9] After that, the Stewart platform gained significant notice as a motion simulator in the first place used for pilot training, and later for training operators in various transportation sectors. The utilization of the Stewart platform enhanced the simulated training effectiveness, while concurrently reducing safety risks and costs of training. Given their significance in industry, numerous research studies in the area of parallel robots have been done to analyzing the various aspects of Stewart robots, including kinematics, dynamics, and optimal design.

Historically, hydraulic actuators have been widely employed in motion simulators until 2006 due to their ability to minimize unwanted vibrations transmitted to the simulator cabin. However, hydraulic systems have several drawbacks, including the need for regular maintenance, costly equipment, susceptibility to oil leakage, and low efficiency.[10,11] In recent years, there has been a shift toward electromechanical motion simulators, which utilize electrical motors as the source of power and give motion to the cabin through ball screws. However, one limitation of electrical simulators is the increased demand for actuator power as the payload weight increases.[12] One of the low-cost solutions for this is the optimization of the designed parameter of the Stewart robot that is done in this study.

The inverse dynamic problem of conventional Stewart platforms has been addressed through diverse methodologies, including Newton-Euler,[13,14] Euler-Lagrange,[15–17] the principle of virtual work,[18–20] and Kane[21] methods. These methods have been utilized to solve the inverse dynamic problem and obtain accurate and reliable solutions. To detect an optimum Stewart Platform, optimization techniques such as particle swarm optimization Algorithm (PSO), and Genetic Algorithm (GA) were used, each of which concentrating on a different specific standard.[22,23] Shariatee and Akbarzadeh[24] focuses on investigating the dynamics and kinematics of a six-axis FUM Stewart robot equipped with three passive redundant pneumatic actuators. By defining six independent routes based on the most allowable velocity and accelerations, the route with the highest force of actuator is identified. A Genetic Algorithm is then employed to optimize consumption of the power for this worst-case route. For minimizing the absolute values of both average and maximum force of actuator, a cost function is formulated by considering the structural kinematics formation of the passive pneumatic actuators. The experimental findings demonstrate that the implemented weight compensation approach successfully reduces actuator forces in both static positions and dynamic trajectories, achieving reductions of at least 29% and 37.1%, respectively.

PSO is inspired by the social behavior of bird flocking or fish schooling, where individuals (particles) cooperate and communicate to find the best solution collectively. This collaborative approach often leads to faster convergence and effective global optimization. PSO tends to converge faster than GA due to its simpler mechanism of updating particle positions based on personal and global best solutions. PSO is computationally less intensive than DE and can handle highdimensional optimization problems effectively. An enhanced particle swarm optimization (PSO) algorithm was presented for investigating the forward kinematics of a solar exploring device with one translational and two rotational DOF. By formulating the parallel manipulator forward kinematics as an optimization issue, the equations of inverse kinematics are solved. The results confirm the feasibility and superiority of the improved way. Furthermore, the performance of the suggested method is examined with floating social and cognitive parameters and a constant value, demonstrating its fast convergence speed.[25] The determination of the forward kinematics of the Stewart robot is important for achieving precise sensation and positioning in 6-DOF. To enhance the convergence speed and address the issue of local convergence, a combined approach of Simulated Annealing (SA) and Particle Swarm Optimization (PSO) is proposed. The SA-PSO algorithm speed up the convergence and enhances the success rate and reliability of the solution. In comparison to the method of NewtonRaphson, the SA-PSO method exhibits a better success rate and requires short time. Eventually, an experiment is done on a 6-DOF platform, demonstrating the reliability and accuracy of the proposed algorithm.[26] Shirazi et al.[27] undertook the simultaneous optimization of three key performance parameters of a parallel manipulators (PM), namely workspace, condition number, and stiffness. Given the complexity inherent in the cost function and the multitude of variables involved, the selection of a robust optimization method capable of converging to the optimal solution assumes paramount importance. Therefore, the particle swarm optimization (PSO) method is used as the optimization framework of choice, demonstrating its efficacy in facilitating the performance optimization of PMs. Kucuk[28]

addressed an optimization challenge concerning the 3-degrees-offreedom RRR fully planar parallel manipulator (3-RRR) with a focus on minimizing actuator power consumption. The optimization objective revolves around determining the optimal masses of the links and platform to minimize the electrical energy expended by the actuators while adhering to stringent kinematic, geometric, and dynamic constraints. Leveraging the Particle Swarm Optimization (PSO) algorithm, renowned for its effectiveness in diverse engineering applications, this study employs it as the optimization tool to tackle the complex mass optimization problem. The Particle Swarm Optimization (PSO) algorithm is employed as a learning algorithm to teach a neural network to predict the forward kinematics of a parallel robot. By utilizing the PSO algorithm, the teaching process is characterized by less time requirements and higher precision.[29] Aldeen Joumah and Albitar[30] presented a comprehensive study focusing on the design optimization of the 6-RUS Stewart platform, employing a novel hybrid algorithm approach. Noteworthy is the comparative analysis of the convergence performance of the genetic algorithm (GA) and the particle swarm optimization (PSO), revealing the superior performance of the PSO algorithm. Farooq et al.[31] optimized the Tricept mechanism through genetic algorithms to enhance its performance metrics. In a bid to augment existing research endeavors, this study introduces the Weighted Particle Swarm Optimization (PSO) technique for multi-objective optimization, offering a comparative analysis with previous optimization methodologies. The outcomes derived from the Weighted PSO technique are meticulously scrutinized, validated, and juxtaposed against published optimization results, thereby enriching the body of knowledge surrounding the optimization strategies employed for the Tricept mechanism. Kumar et al.[32] study is centered on path planning utilizing a cubic spline approach, augmented by a layer of intelligence through the integration of the particle swarm optimization (PSO) algorithm. The research endeavors to enhance path planning efficiency by leveraging the PSO algorithm, a computational optimization technique known for its ability to navigate complex problem spaces effectively. By introducing the PSO algorithm to the realm of path planning, this study aims to facilitate the identification of the optimal shortest path between two specified terminal points. This innovative approach amalgamating PSO with path planning holds promise for optimizing pathfinding processes and improving navigation outcomes in scenarios characterized by dynamic environments and spatial constraints.

In this survey, the kinematic, velocity, and acceleration analysis of a Stewart platform are investigated. Then, dynamic equations are extracted by utilizing the method of Newton-Euler. Then a general Stewart platform with a particular property was studied to calculate the required performance specifications of the electric actuators to provide the desired trajectory. Finally, with the PSO algorithm, different design parameters for the Stewart robot are simulated and compared to minimize the maximum speed and maximum Force of the prismatic actuators. As a result of design parameters optimization, the maximum actuator power was reduced and consequently, the Stewart platform's life increased. The novelty of this study lies in its pioneering approach toward optimizing the Dynamic Parameter Design of a Stewart Platform through the utilization of the Particle Swarm Optimization (PSO) Algorithm. Prior to this investigation, the optimization of dynamic parameters for Stewart Platforms with the PSO Algorithm had not been explored, signifying a significant gap in the existing literature. By introducing this novel methodology, the study aims to address this lacuna and contribute valuable insights into the realm of dynamic parameter optimization for Stewart Platforms, thereby paving the way for new avenues of research in the field of parallel manipulators.

Stewart structure features

A Stewart robot's structure can be defined based on five parameters listing in Table 1 and shown in Figure 1.

The optimization process is used to select the parameters for the Stewart robot, with consideration given to the payload specification and desired trajectories such as workspace, velocity, and acceleration during the design process.

Inverse kinematic analysis

The inverse kinematics of the 6-UPS Stewart platform involve relating the properties of the joint to the position and orientation of the end effector and also, determining the actuator lengths required to achieve a desired position and orientation of the end effector.

Table 1. Parameters of Stewart robot's structure.

Design parameter	Description
R_b	Circle radius passes from the universal joints on the base platform
γ_b	Half of the angle among two near universal joints on the base platform
R_p	Circle radius passes from the spherical joints on the moving platform
γ_p	Half of the angle among two near spherical joints on the moving platform
Z_S	Distance between base platforms and moving platform (neutral height)

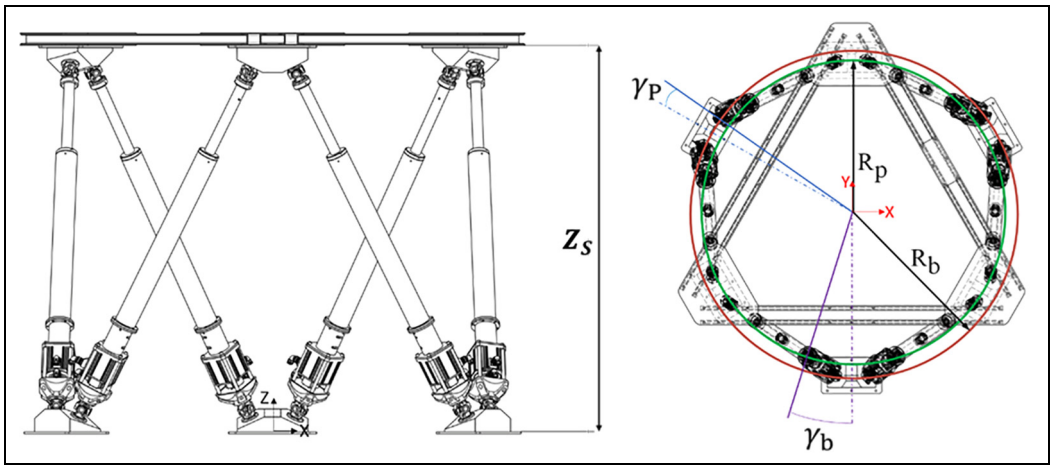

Figure 1. Geometrical design parameters of Stewart platform.

The standard approach to the joint variable involves creating a closed loop that connects the base coordinates $\{X_0, Y_0, Z_0\}$, to the moving platform coordinates, $\{X_M, X_M, Z_M\}$, and solving for each chain. The electric robot legs and a standard kinematic chain of the Stewart robot are shown in Figure 2. The base coordinate system is used to define position vectors of the base universal joints and end-effector as $\vec{B}_i$ and $\vec{M}$ respectively. In addition, spherical joints position relative to the moving coordinates is represented by $\overrightarrow{SP}_{iM}$.

The solution of inverse kinematics can provide the length vector of the i_{th} actuator, $\vec{L}_i$, through equation (1).

$$\vec{L}_i = \vec{M} + \mathcal{R}\,\overrightarrow{SP}_{iM} - \vec{B}_i \tag{1}$$

where $\mathcal{R}$ is the rotation matrix of the moving end effector from the base. To obtain the rotation matrix of the moving coordinate, a ZYX Euler angle representation is implemented. To determine the direction of each actuator, the length vector is divided by its length value to obtain the unit vector $\vec{A}_i$ as equation (2).

$$\vec{A}_i = \frac{\vec{L}_i}{||\vec{L}_i||} \tag{2}$$

This is a 6-UPS robot, or generally, an n-UPS and $i = 1$–6 for $\vec{L}_i$.

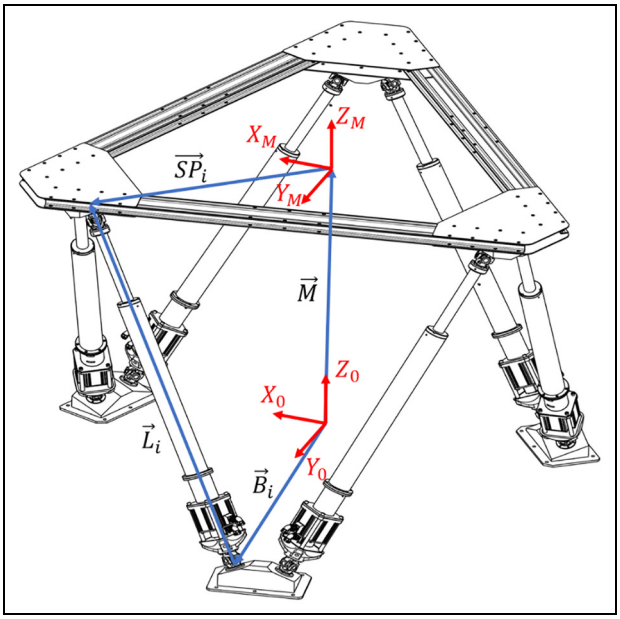

Figure 2. The electric robot legs and a standard kinematic chain of the Stewart robot.

Velocity and acceleration analysis

To obtain the velocity and acceleration of the moving parts of the 6-UPS Stewart platform, the equations of the actuator length vectors are differentiated with respect to time. This allows for the calculation of the Jacobian matrix, which relates the velocities of the prismatic legs to the velocities of the end effector. The methodology employed for analyzing acceleration is similar with that used for velocity analysis. These analyses enable the determination of the position, velocity, and acceleration components of the prismatic legs when the end effector predetermined trajectory is given. The Jacobian matrix establishes the relationship between the twist vector of the end effector and the velocities of the joints. The time derivation of the equation (1) is given by the equation (3).

$$\dot{L}_i\vec{A}_i + L_i(\vec{\omega}_i \times \vec{A}_i) = \dot{\vec{M}}_i \quad + \vec{\in} \times \mathcal{R}\,\overrightarrow{SP}_{iM} \tag{3}$$

where $\vec{\omega}_i$ is angular velocities of the i_{th} leg and $\vec{\in}$ represent angular velocities of the moving platform. In order to map velocity from the Cartesian space that is,

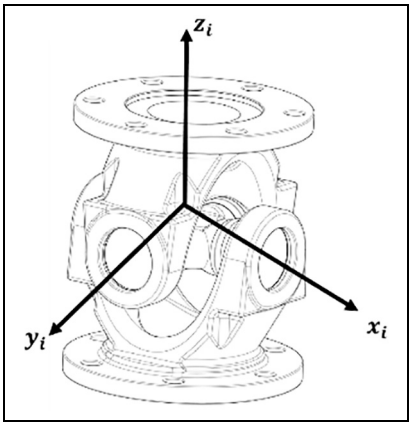

Figure 3. Coordinate frame of universal joint.

$\vec{V}_{tot} = \begin{bmatrix} \vec{V}^T & \vec{\in}^T \end{bmatrix}^T$, to joint space that is, $\dot{L}_i = \begin{bmatrix} \dot{L}_1 & \dot{L}_2 & \dot{L}_3 & \dot{L}_4 & \dot{L}_5 & \dot{L}_6 \end{bmatrix}^T$, equation (3) dot product by $\vec{A}_i$ give equation (4).[24]

$$\dot{L}_i = J_V \vec{V}_{tot} \tag{4}$$

J_V, Jacobian matrix can be expressed as equation (5).

$$J_V = \begin{bmatrix} \vec{A}_1^{\,T} & (\mathcal{R}\overrightarrow{SP}_{iM} \times \vec{A}_1)^T \\ \vec{A}_2^{\,T} & (\mathcal{R}\overrightarrow{SP}_{iM} \times \vec{A}_2)^T \\ \vec{A}_3^{\,T} & (\mathcal{R}\overrightarrow{SP}_{iM} \times \vec{A}_3)^T \\ \vec{A}_4^{\,T} & (\mathcal{R}\overrightarrow{SP}_{iM} \times \vec{A}_4)^T \\ \vec{A}_5^{\,T} & (\mathcal{R}\overrightarrow{SP}_{iM} \times \vec{A}_5)^T \\ \vec{A}_6^{\,T} & (\mathcal{R}\overrightarrow{SP}_{iM} \times \vec{A}_6)^T \end{bmatrix} \tag{5}$$

If consider a general coordinate for the end effector as, $x = [x, y, z, \phi, \theta, \psi]^T$, mapping of velocity between general coordinate and joint space could be written by J_x as equation (6)[24]:

$$\dot{L}_i = J_x \dot{\vec{x}} \qquad J_x = J_V J_E \tag{6}$$

In equation (6) choose Euler formulation Jacobian, J_E, based on the Euler angles, as equation (7).

$$J_E = \begin{bmatrix} 1 & 0 & 0 & 0 & 0 & 0 \\ 0 & 1 & 0 & 0 & 0 & 0 \\ 0 & 0 & 1 & 0 & 0 & 0 \\ 0 & 0 & 0 & \cos\psi\cos\theta & -\sin\psi & 0 \\ 0 & 0 & 0 & \sin\psi\cos\theta & \cos\psi & 0 \\ 0 & 0 & 0 & -sin\theta & 0 & 1 \end{bmatrix} \tag{7}$$

In order to determine the moving parts acceleration, a similar approach for analyzing velocity has been employed. Consequently, the equation (1) has been acquired as equation (8).

$$\ddot{L}_i\vec{A}_i + 2\dot{L}_i(\vec{\omega}_i \times \vec{A}_i) + L_i(\vec{\alpha}_i \times \vec{A}_i) + L_i(\vec{\omega}_i \times (\vec{\omega}_i \times \vec{A}_i)) = \ddot{\vec{M}} + \dot{\vec{\in}} \times \mathcal{R}\overrightarrow{SP}_{iM} + \vec{\in} \times (\vec{\in} \times \mathcal{R}\overrightarrow{SP}_{iM}) \tag{8}$$

This equation includes various terms such as angular accelerations of the moving platform and i_{th} leg denoted as $\vec{\alpha}_i$ and $\dot{\vec{\in}}$ respectively. In equations (3) and (8) angular acceleration and velocity of legs are unknown. The universal joint coordinate frame is shown in Figure 3 and, $\vec{\omega}_i$ is obtained following the instruction in Nabavi et al.[33,34]

Cause of all prismatic leg can rotate about $\vec{x}_i$ and $\vec{y}_i$ axes, equations (9)–(11) provide $\vec{\omega}_i$ by its constituting components as[24]:

$$\vec{\omega}_i = \omega_{xi}\vec{x}_i + \omega_{yi}\vec{y}_i \tag{9}$$

$$\omega_{xi} = -\frac{(\dot{\vec{L}}_i - \dot{L}_i\vec{A}_i).\vec{y}_i}{L_i(\vec{A}_i.\vec{z}_i)} \tag{10}$$

$$\omega_{yi} = \frac{(\dot{\vec{L}}_i - \dot{L}_i\vec{A}_i).\vec{x}_i}{L_i(\vec{A}_i.\vec{z}_i)} \tag{11}$$

The Time derivative of the equations (9)–(11) obtain the legs angular acceleration as equations (12)–(14).[24]

$$\vec{\alpha}_i = \alpha_{xi}\vec{x}_i + \alpha_{yi}\vec{y}_i + \omega_{xi}\omega_{yi}\vec{z}_i \tag{12}$$

$$\alpha_{xi} = -\frac{\vec{\beta}_i.\vec{y}_i}{L_i(\vec{A}_i.\vec{z}_i)} \tag{13}$$

$$\alpha_{yi} = \frac{\vec{\beta}_i.\vec{x}_i}{L_i(\vec{A}_i.\vec{z}_i)} \tag{14}$$

Where $\vec{\beta}_i$ obtained by equation (15)[24]:

$$\vec{\beta}_i = \ddot{\vec{L}}_i - (\ddot{L}_i\vec{A}_i + \vec{\omega}_i \times (\vec{\omega}_i \times \vec{L}_i) + 2\vec{\omega}_i \times \dot{L}_i\vec{A}_i + \omega_{xi}\omega_{yi}L_i(\vec{z}_i \times \vec{A}_i)) \tag{15}$$

By solving this section's equations, the prismatic legs position, velocity, and acceleration can be determined based on a end effector predetermined trajectory.

Dynamic of Stewart robot

The primary aim of the inverse dynamic analysis is to specify the actuator forces necessary to produce motion along a desired trajectory. The data gathered from the previous section, encompassing positional, velocity, and acceleration analyses, serves as the foundation for deriving the dynamic equations. Subsequently, the effective forces exerted by the actuators are determined through the solution of these dynamic equations.

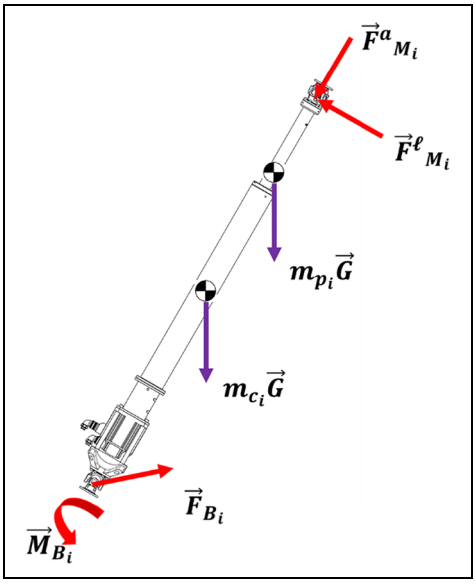

Figure 4. The electric actuator free body diagram.

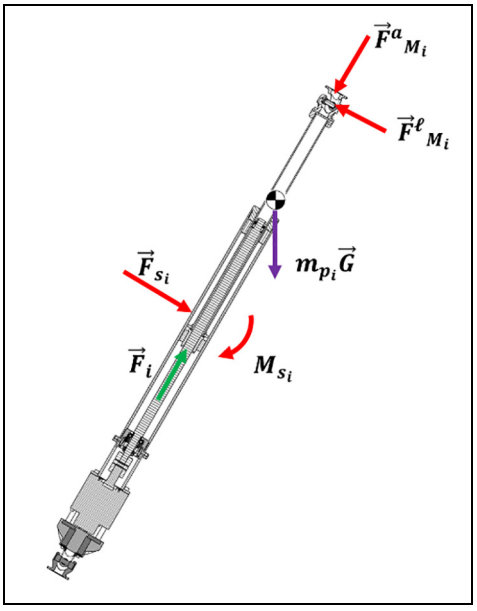

Figure 5. The piston rod of prismatic leg free body diagram.

Table 2. Inertia tensor, mass, position vectors, acceleration vectors, and the gravitational vector of the electric actuator.

Equation terms	Description
m_{c_i}	Prismatic leg's cylinder mass
m_{p_i}	Prismatic leg's piston mass
$\vec{r}_{c_i}$	Prismatic leg's cylinder center of mass position vectors
$\vec{r}_{p_i}$	Prismatic leg's piston center of mass position vectors
$\bar{I}_{c_i}$	Prismatic leg's cylinder inertia tensor about principal axes
$\bar{I}_{p_i}$	Prismatic leg's piston inertia tensor about principal axes
$\vec{a}_{ci}$	Leg's cylinder center of mass acceleration vectors
$\vec{a}_{pi}$	Leg's piston center of mass acceleration vectors
$\vec{G}$	The gravitational vector $\vec{G} = [0, 0, -9.81]^T$

Robot legs dynamic

Utilizing the Newton-Euler for solving the equation of dynamic, the initial step involves constructing free-body diagrams for each individual part. The moving platform and the electric actuator are moving parts of robot. Figure 4 illustrates the electric actuator free-body diagrams. The moving platform exert $\vec{F}^{a}{}_{M_i}$ for component of axial force and $\vec{F}^{\ell}{}_{M_i}$ for component of lateral force on the prismatic legs as reaction forces. By the same written, $\vec{F}_{B_i}$ shows the base platform reaction force. Additionally, a reaction moment, $\vec{M}_{B_i}$, arises due to the limitations of universal joints that restrict rotation about the zi axis.[24]

Referring to Figure 4, the electric actuator Euler equation in terms of the universal joint center is determined by equation (16).

$$\vec{M}_{Bi} + m_{c_i}\vec{r}_{c_i} \times \vec{G} + m_{p_i}\vec{r}_{p_i} \times \vec{G} + L_i\vec{A}_i \times \vec{F}^{\ell}{}_{M_i} = (\bar{I}_{c_i} + \bar{I}_{p_i})\vec{\alpha}_i + \vec{\omega}_i \times ((\bar{I}_{c_i} + \bar{I}_{p_i})\vec{\omega}_i) + m_c\vec{r}_{ci} \times \vec{a}_{ci} + m_p\vec{r}_{p_i} \times \vec{a}_{pi} \tag{16}$$

This equation incorporates various terms such as the inertia tensor, mass, position vectors, acceleration vectors, and the gravitational vector given in Table 2.

The dot product of equation (16) and $\bar{A}i$ and also its cross product, respectively is represented in equations (17) and (18). Consequently, reaction moment and lateral force for the prismatic leg are expressed as equations (17)–(19).[24]

$$\vec{M}_{Bi} = \frac{\vec{N}_i.\vec{A}_i}{\vec{A}_i.\vec{z}_i}\vec{z}_i \tag{17}$$

$$\vec{F}^{\ell}{}_{M_i} = \frac{1}{L}(\vec{N}_i - \vec{M}_{Bi}) \times \vec{A}_i \tag{18}$$

$$\vec{N}_i = (\bar{I}_{c_i} + \bar{I}_{p_i})\vec{\alpha}_i + \vec{\omega}_i \times ((\bar{I}_{c_i} + \bar{I}_{p_i})\vec{\omega}_i) + m_c\vec{r}_{c_i} \times \vec{a}_{c_i} + m_p\vec{r}_{p_i} \times \vec{a}_{p_i} - m_c\vec{r}_{c_i} \times \vec{G} - m_p\vec{r}_{p_i} \times \vec{G} \tag{19}$$

The rod piston of the actuator inner forces are depicted in Figure 5. The force required for piston moving in the up and down directions is signified as F_i. M_{s_i} and F_{s_i} represent piston rod moment and force which is reaction of the cylinder wall, respectively.

Motion of the piston of the legs which is acquired by Newton equation is given by equation (20).

$$\vec{F}_i + \vec{F}^a{}_{M_i} + \vec{F}^\ell{}_{M_i} + \vec{F}_{s_i} + m_{p_i}\vec{G} = m_{p_i}\vec{a}_{p_i} \tag{20}$$

Equation (20) seeks to determine the forces in the direction of the axis of the piston. By taking the dot product of equation (20) with A⃗i, the vectors normal component of would be eliminated.

Dynamic of platform

For moving platform dynamic analyzing, the moving platform including payload free-body diagram is depicted in Figure 6. The whole of the moving load includes of the payload and mass of platform, with relevant terms denoted by the subscript (tot). $\bar{I}_{tot}$ shows all moving load inertia and M_{tot} represent the total mass. The $\vec{r}_{tot}$ is vector of position and indicates mass center of the moving loads distance from the coordinate of the moving frame.

The equations of Newton-Euler governing the whole moving load about the origin of the coordinate of the moving frame are expressed in equations (21) and (22).[24]

$$M_{tot}\vec{G} - \sum_{i=1}^{6}\vec{F}^{a}{}_{M_i} - \sum_{i=1}^{6}\vec{F}^{\ell}{}_{M_i} + \vec{F}_{ext} = M_{tot}\vec{a}_{tot} \tag{21}$$

$$M_{tot}\vec{r}_{tot}\times\vec{G} - \sum_{i=1}^{6}(\mathcal{R}\vec{s}_i\times\vec{F}^{a}{}_{M_i}) - \sum_{i=1}^{6}(\mathcal{R}\vec{s}_i\times\vec{F}^{\ell}{}_{M_i}) + \vec{M}_{ext} + \vec{r}_{tot}\times\vec{F}_{ext} = \bar{I}_t\dot{\vec{\epsilon}} + \vec{\epsilon}\times\bar{I}_t\vec{\epsilon} + M_t\vec{r}_{tot}\times\vec{a}_{tot} \tag{22}$$

where $\vec{a}_{tot}$ is the whole moving load acceleration vector, and respectively, $\vec{M}_{ext}$ and $\vec{F}_{ext}$ are the applied moment and outer force on the whole moving load. Matrix form of combined equations (21) and (22) is equation (23).

$$J^{T}_{V(1-6\times 1-6)}\vec{F}^{a}{}_{M} = \vec{W} \tag{23}$$

Where, $J_{V(1-m\times 1-n)}$ shows a matrix derived from the first m rows and n columns of matrix J_V, and $\vec{F}^a{}_M$ is $[f^a{}_{M1}\ f^a{}_{M2} f^a{}_{M3} f^a{}_{M4}\ \ f^a{}_{M5}\ \ f^a{}_{M6}]^T$ in which $f^a{}_{M_i}$ is the magnitude of $\vec{F}^a{}_{M_i}$.[24] Furthermore, $\vec{W}$ encompasses moments and outer and inner forces, as defined in equation (24). previously, $\vec{W}$ all terms have been acquired.

$$\vec{W} = \begin{bmatrix} M_{tot}\left(\vec{G} - \vec{a}_{tot}\right) - \sum_{i=1}^{6}\vec{F}^{\ell}{}_{M_i} + \vec{F}_{ext} \\ M_{tot}\vec{r}_{tot}\times(\vec{G} - \vec{a}_{tot}) - \bar{I}_{tot}\dot{\vec{\epsilon}} - \vec{\epsilon}\times\bar{I}_{tot}\vec{\epsilon} \\ \quad - \sum_{i=1}^{6}(\mathcal{R}\overrightarrow{SP}_{iM}\times\vec{F}^{\ell}{}_{M_i}) + \vec{M}_{ext} + \vec{r}_{tot}\times\vec{F}_{ext} \end{bmatrix} \tag{24}$$

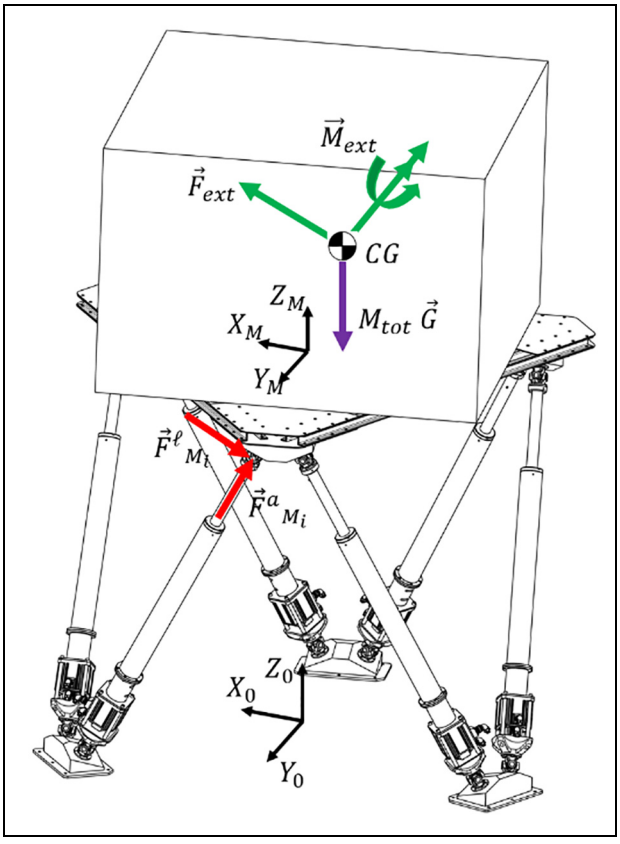

Figure 6. The moving platform with the payload free body diagram.

Equations (18) and (23) are utilized for obtaining $\vec{F}_M$. Additionally, The dot product of $\vec{A}_i$ and equation (25) gives the equation (20) scalar format. Consequently, the electric actuators driving force is determined.

$$||\vec{F}_i|| + ||\vec{F}^a{}_{M_i}|| + m_{p_i}\vec{G}.\vec{A}_i = m_{p_i}\vec{a}_{p_i}.\vec{A}_i \tag{25}$$

Simulation

Within the motion simulation field, distinct nomenclature is assigned to movements along individual degrees of freedom. As such, trajectories occurring along the X, Y, and Z axes are denoted as Surge, Sway, and Heave, respectively. Conversely, trajectories revolving around the X, Y, and Z axes are referred to as Roll, Pitch, and Yaw, correspondingly. This standardized naming convention facilitates clear and consistent communication within the industry, enabling precise descriptions and analysis of motion patterns in various applications.

A dynamic simulation was conducted on a Stewart platform with specifications provided in Table 3. The simulation was performed using the Maplesim software. One of the objectives of this simulation is to verify the dynamic equations. The additional intention for dynamic simulation is to calculate the required

Table 3. Specifications of Stewart platform.

Design parameter	Value
R_b	3.3 m
γ_b	3 deg
R_p	3 m
γ_p	3 deg
Z_S	2.3 m
I_x, I_y, I_z of platform	5000 kg m^2
Mass of platform	5000 kg

Table 4. Desired trajectory of the Stewart platform.

Desired trajectory	Value
Angular workspace in roll, pitch, and yaw axis	± 45 deg
Maximum angular velocity in roll and pitch axis	± 250 deg/s
Maximum angular acceleration in roll and pitch axis	± 600 deg/s^2
Maximum angular velocity in yaw axis	± 160 deg/s
Maximum angular acceleration in yaw axis	± 1200 deg/s^2

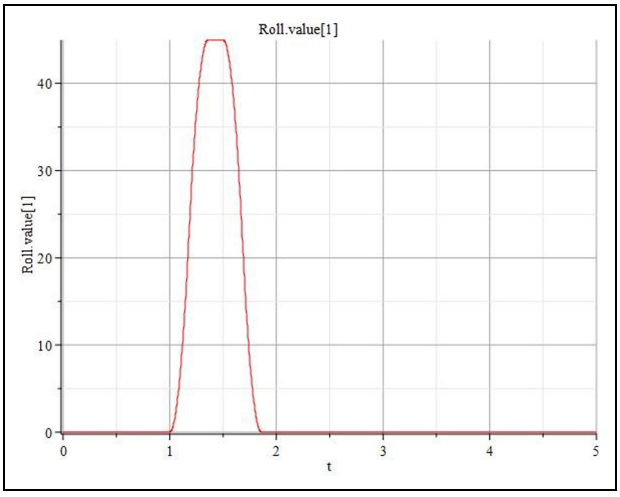

Figure 7. Graph of desired angle changes (deg) along the Roll axis in the time domain.

performance specifications of the electric actuator to provide the necessary dynamic conditions in Table 4.

Initially, dynamic movements are carried out from the zero position of the Stewart platform to the desired degree position, based on the maximum requested speed and acceleration in Table 4. The Stewart platform then returns to the zero position at the same speed and acceleration. This process is performed along a desired trajectory within 5 s. The graph of the Stewart platform's desired trajectory in Roll, Pitch, and Yaw is illustrated in Figures 7 to 15.

By applying these desired trajectories on the Stewart platform with specifications provided in Table 3, the

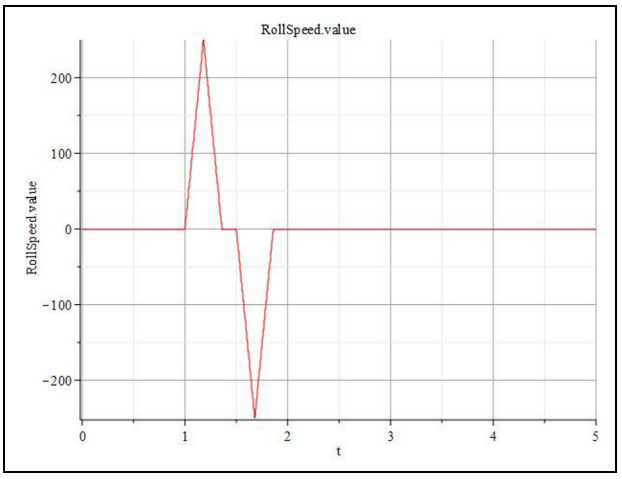

Figure 8. Graph of desired angular velocity changes (deg/s) along the Roll axis in the time domain.

dynamic characteristics of electric actuators, including force, velocity, and actuator displacement, are calculated. The simulation results for each actuator during the desired motion, are illustrated in Figures 16 to 18.

Based on the results, the maximum power required for the actuators can be estimated based on the maximum speed and maximum force of the jacks. In the Stewart platform with specifications reported in Table 3, the instantaneous power required for each actuator can reach up to 360 kW, indicating the inadequacy of these dimensions for high-speed behavior and high rotational workspace. Consequently, the optimization of the Stewart platform according to the performance specifications of the actuators has been conducted. This approach ensures that the platform is designed and configured in a manner that maximizes its efficiency and effectiveness.

Optimization

The Particle Swarm Optimization (PSO) algorithm is a creative optimization technique. It is widely used in solving complex optimization problems due to its simplicity and efficiency. In PSO, a particles population, each showing a potential solution, moves via the search space to find the optimal solution. The particles regulate their positions according to their own best-known solution and the global best-known solution found by any particle in the swarm. This collective movement toward promising regions of the search space enables PSO to effectively explore and exploit the solution space, leading to the identification of near-optimal or optimal solving. The algorithm's ability to handle nonlinear, multimodal, and high-dimensional problems makes it particularly suitable for a wide range of real-world applications in engineering.

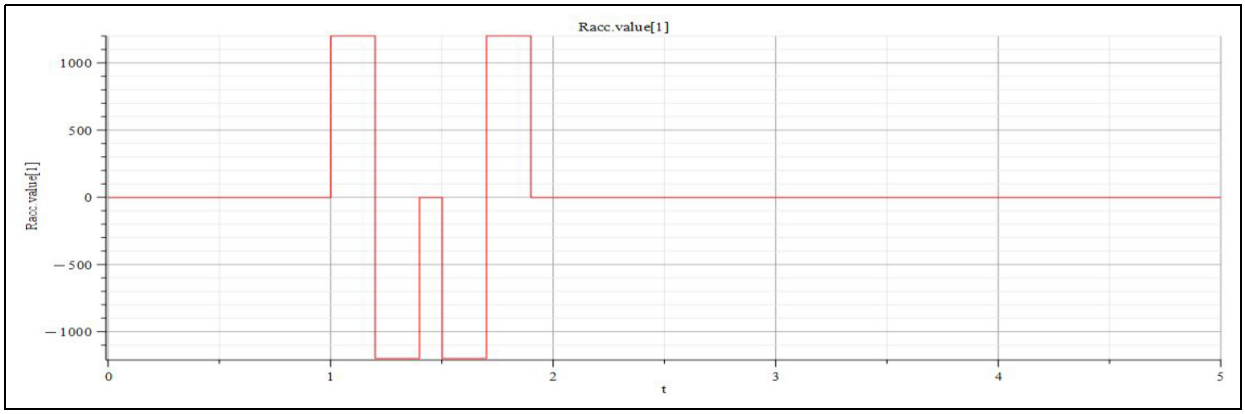

Figure 9. Graph of desired angular acceleration changes (deg/s^2) along the Roll axis in the time domain.

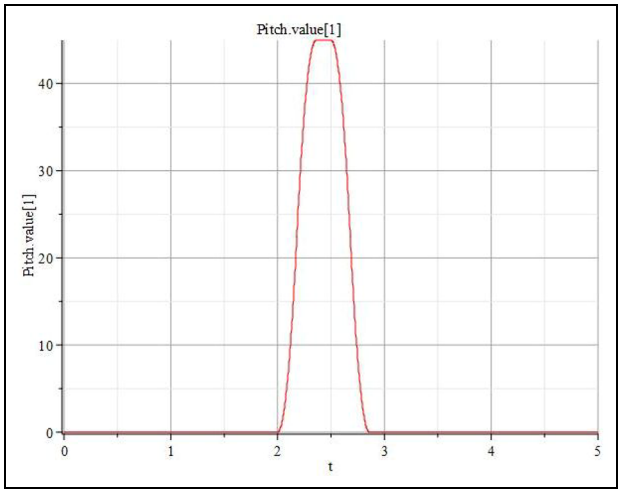

Figure 10. Graph of desired angle changes (deg) along the Pitch axis in the time domain.

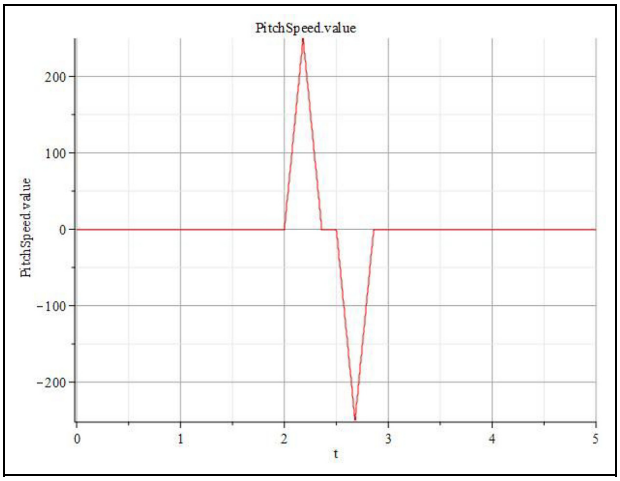

Figure 11. Graph of desired angular velocity changes (deg/s) along the Pitch axis in the time domain.

The aim of optimization of the Stewart platform design parameters based on the performance specifications of the actuators is to decrease the actuator power required for motion simulation and rise the life of the parts. These factors specify cost of the actuator and the power consumption of the robot. To achieve this aim PSO algorithm is utilized for detecting the suitable formation by making modification to parameters of the design are shown in Table 1.

Considering the desired trajectory of the Stewart platform, PSO algorithm try to find a formation, which the Maximum speed and Maximum Force of the jacks tend to get minimized. To satisfy this aim, equation (26), a weighted cost function is defined as follow:

$$Cost\,function = (maximum\,Speed) + (maximum\,Force) \tag{26}$$

δ_1 and δ_2 are the coefficients that are chosen considering the relative importance and impact of each term on the overall optimization goal. Considering optimization goals in this study which are to reduce the required actuator power and increase components' life, Maximum Speed has a significant portion and Maximum Force has a minor portion of the overall optimization goal.

It is necessary to mention that minimum and maximum range of the design parameters provided in Table 5.

In order to perform optimization using the Particle Swarm Optimization (PSO) algorithm, the simulated dynamic model obtained from Maplesim software is used and generate a simulink component block and then implement the PSO code in MATLAB. The number of 1200 simulations are performed on various design parameters, considering the minimum and maximum ranges of the parameters as given in Table 5. Finally, the optimal values are obtained.

The design parameters of the optimized stewart platform based on the defined cost function in equation (26) can be observed in Table 6.

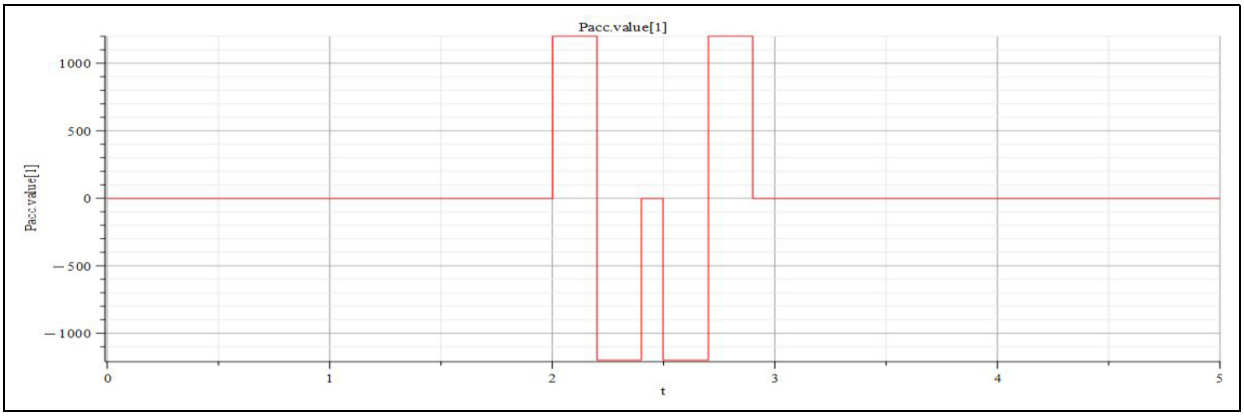

Figure 12. Graph of desired angular acceleration changes (deg/s^2) along the Pitch axis in the time domain.

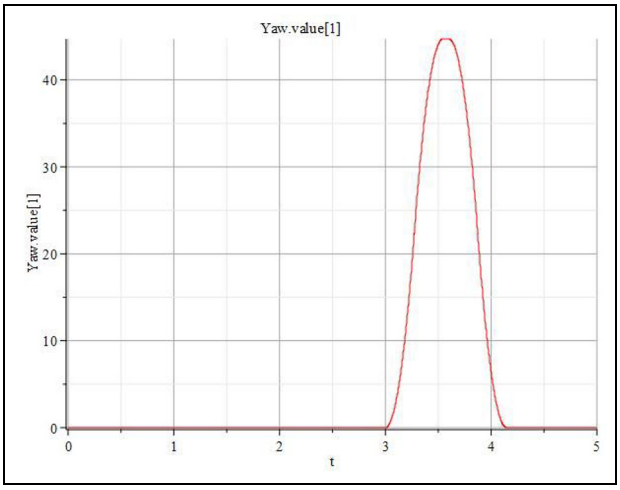

Figure 13. Graph of desired angle changes (deg) along the Yaw axis in the time domain.

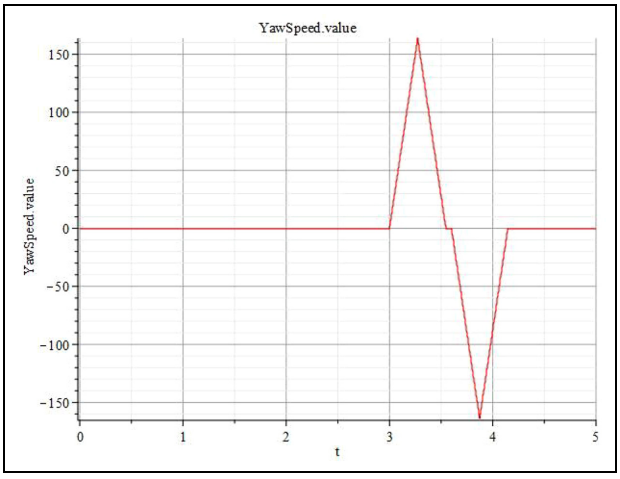

Figure 14. Graph of desired angular velocity changes (deg/s) along the Yaw axis in the time domain.

The simulation results of the optimization are presented in the graphs of Figures 19 to 22.

Based on the analyses, the maximum output performance for Stewart platform electric jacks according to Table 7 is within the normal working range for electric jacks. The maximum Actuator Power from 360 kW was reduced to 42 kW. It is necessary to mention before optimization that these values do not represent the maximum power performance required for the ball screw and electric motor in this particular design, and sufficient safety factors must be considered for the selection of these components in the design process.

Conclusion

In this paper, the effect of optimization (with PSO algorithm) of the design parameters of a general Stewart platform on needed power of the actuator for motion simulation in the desired trajectory has been studied. To this aim, the inverse dynamic analysis is done to determine the actuator forces necessary to produce motion along a desired trajectory. Then, the data gathered from the inverse dynamic, encompassing positional, velocity, and acceleration analyses, serves as the foundation for deriving the dynamic equations. Subsequently, the effective forces exerted by the actuators are determined through the solution of these dynamic equations. Next, a dynamic simulation was conducted on a Stewart platform with a particular property to calculate the required performance specifications of the electric actuators to provide the desired trajectory. Finally, the Particle Swarm Optimization (PSO) algorithm was utilized for optimization of the Stewart platform design parameters. A weighted cost function is defined to find a layout in which the maximum speed and maximum Force of the jacks tend to be minimized. Based on the outputs, the maximum actuator power decline was 88.3% for the desired trajectory and consequently, increased the Stewart

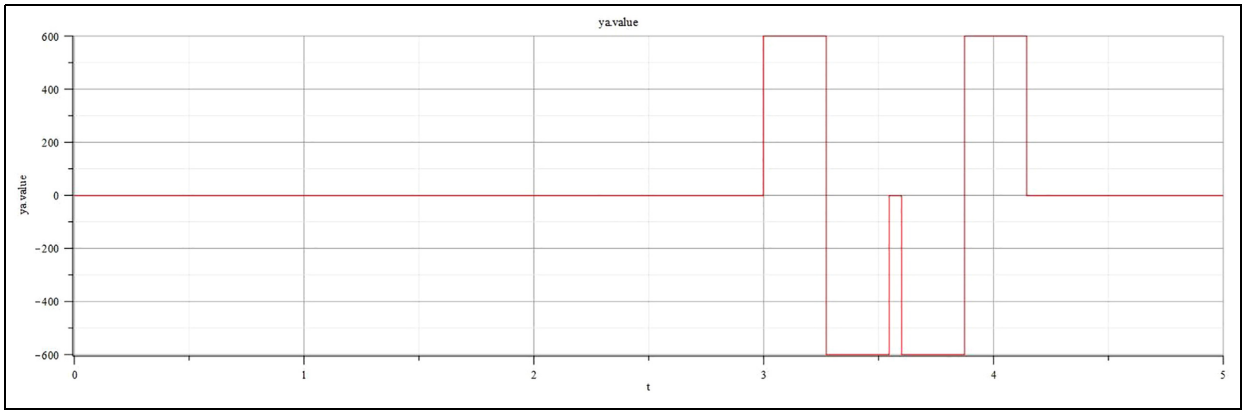

Figure 15. Graph of desired angular acceleration changes (deg/s^2) along the Yaw axis in the time domain.

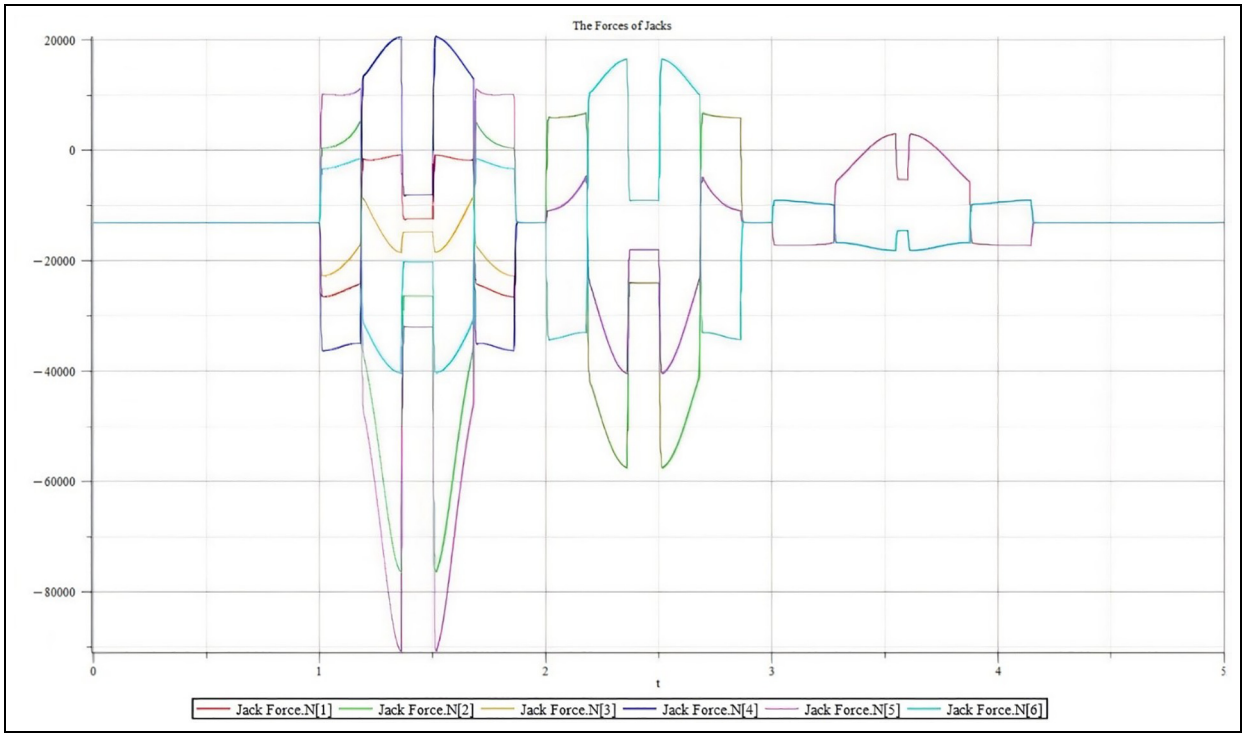

Figure 16. Graph of jacks force changes (N) in the time domain.

Table 5. Minimum and maximum range of the design parameters.

Range of parameter	Z_S	R_p	R_b	γ_p	γ_b
Minimum range	0.6	0.25	0.25	2	2
Maximum range	2.5	1.5	2.5	50	50

Table 6. Optimized design parameters of the Stewart platform.

Design parameter	Value
R_b	1.72 m
γ_b	3 deg
	0.5 m
γ_p	13 deg
Z_S	2.5 m

platform' life. The current study in this paper has the potential for integrating any Stewart simulators with any desired trajectory and weighted cost function to remarkably modify their efficiency of the power consumption and increase their life of the mechanical parts.

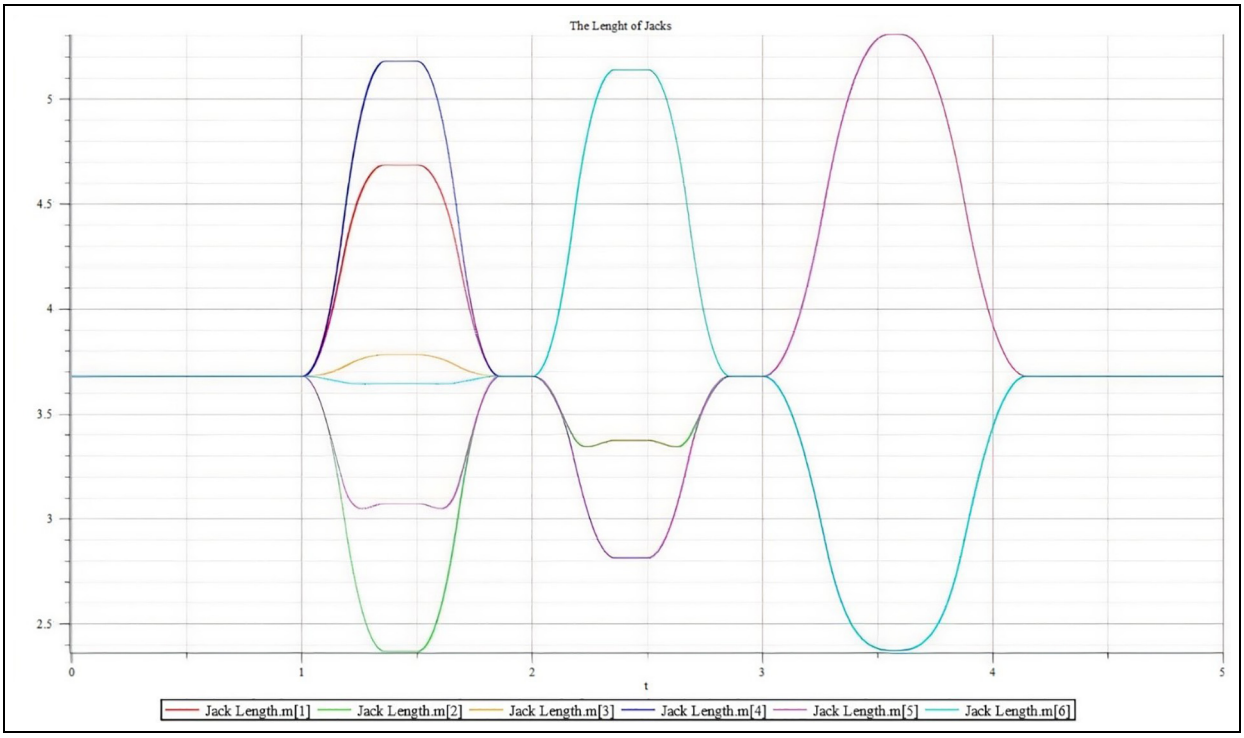

Figure 17. Graph of jacks length changes (N) in the time domain.

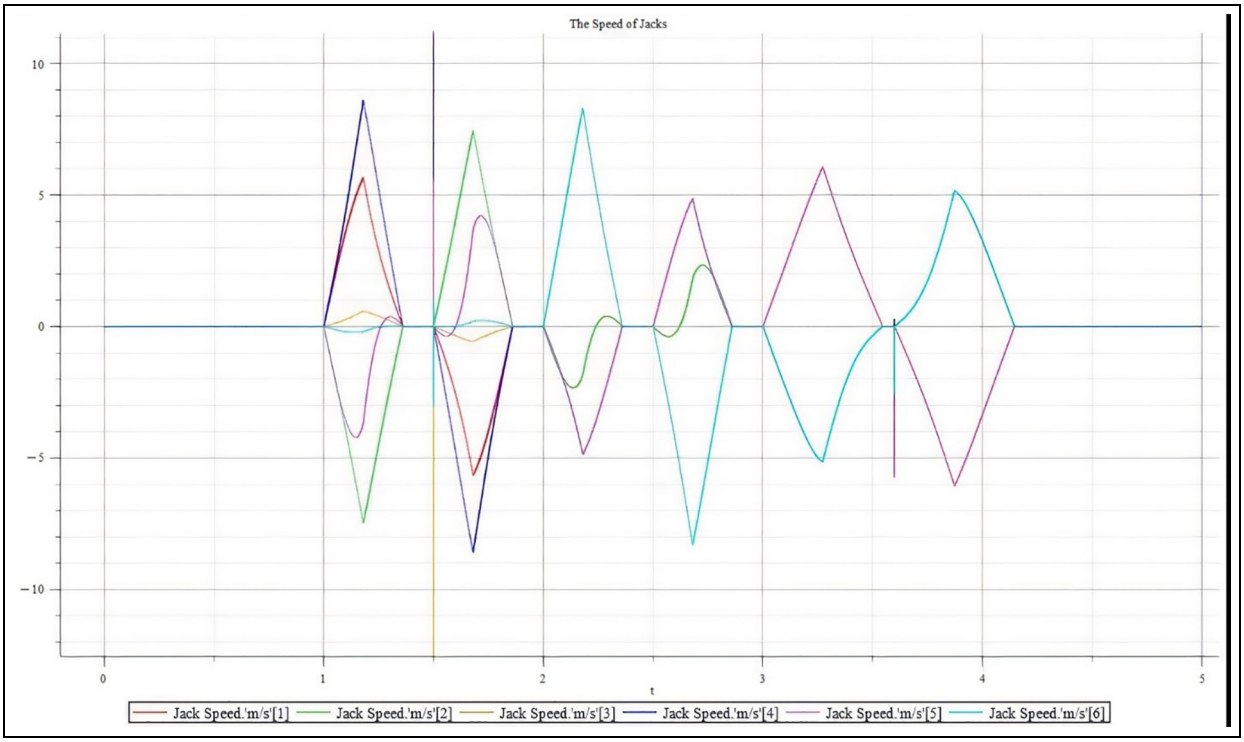

Figure 18. Graph of jacks speed changes (N) in the time domain.

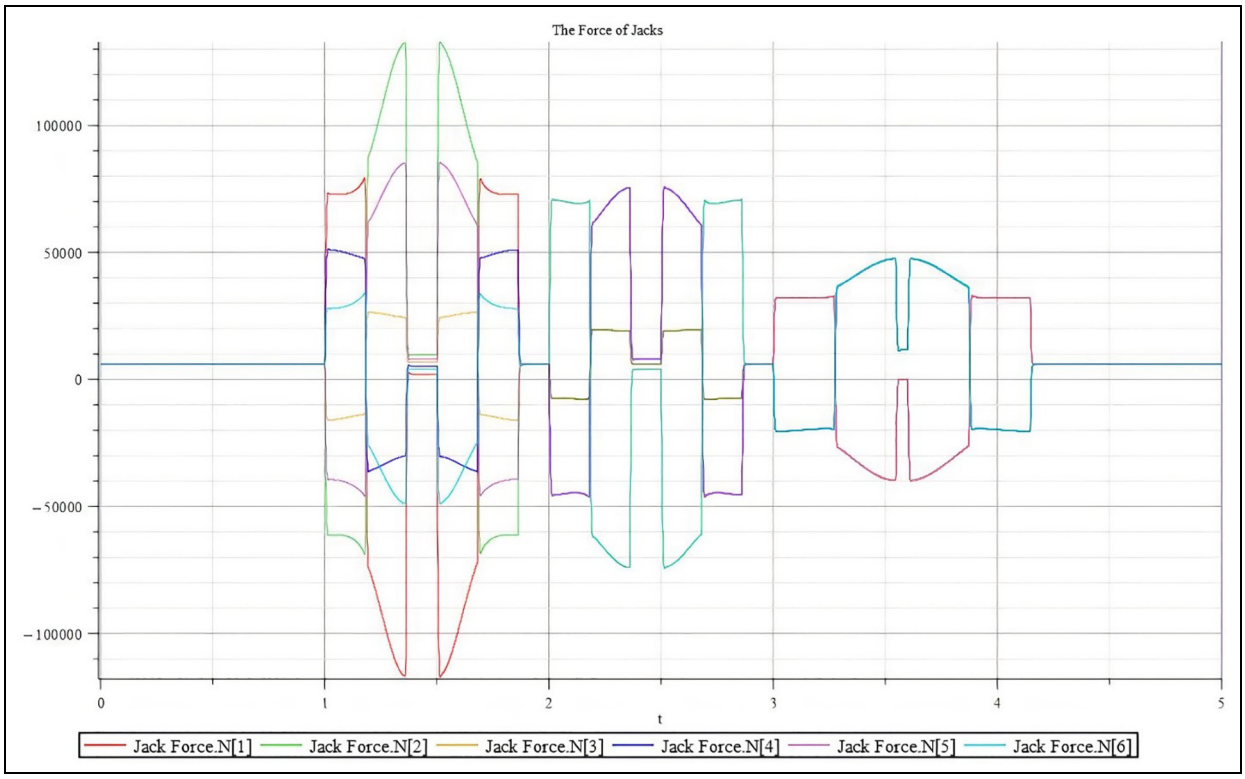

Figure 19. Graph of optimized jacks force (N) in the time domain.

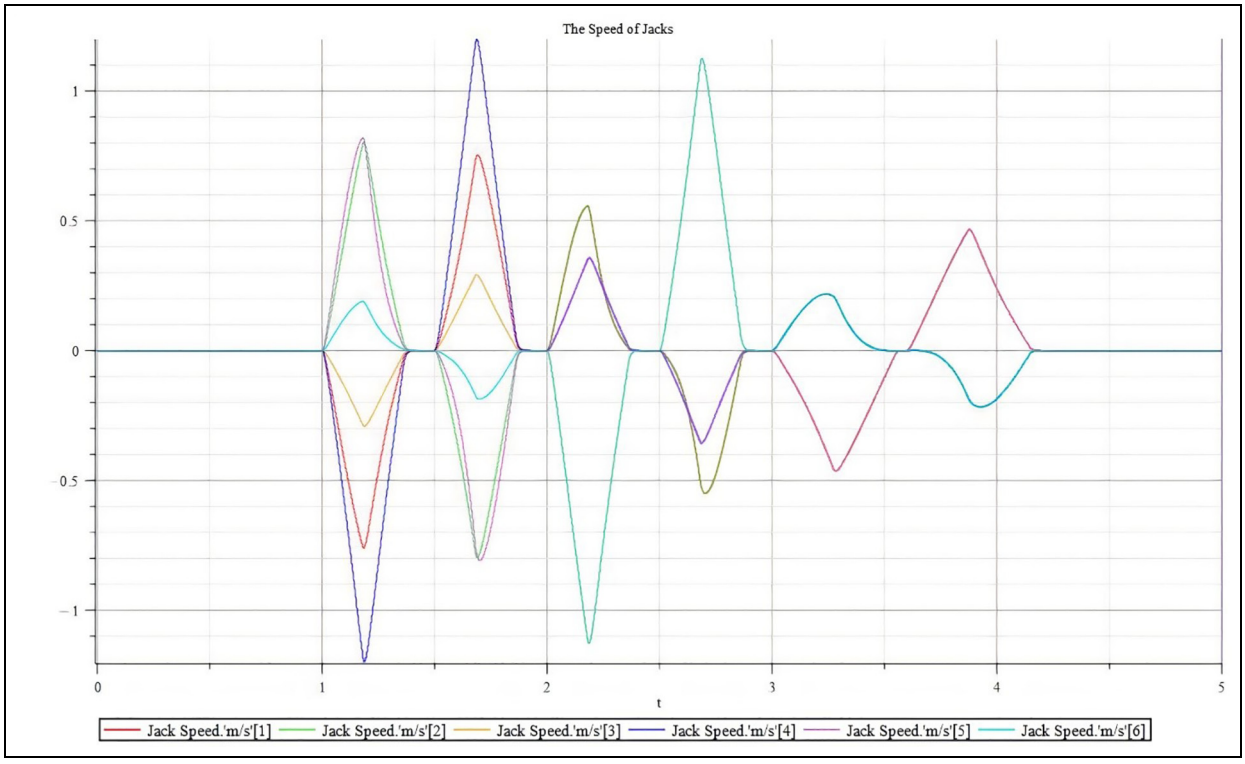

Figure 20. Graph of optimized jacks speed (m/s) in the time domain.

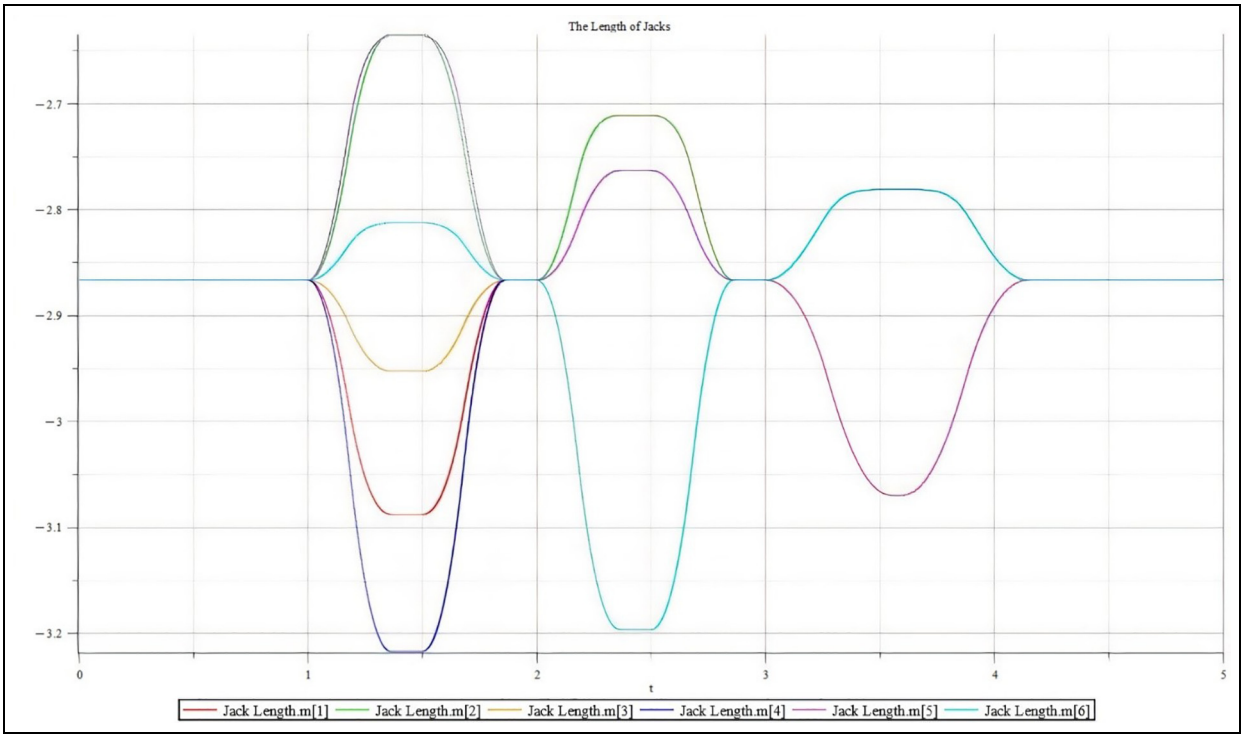

Figure 21. Graph of optimized jacks length (m) in the time domain.

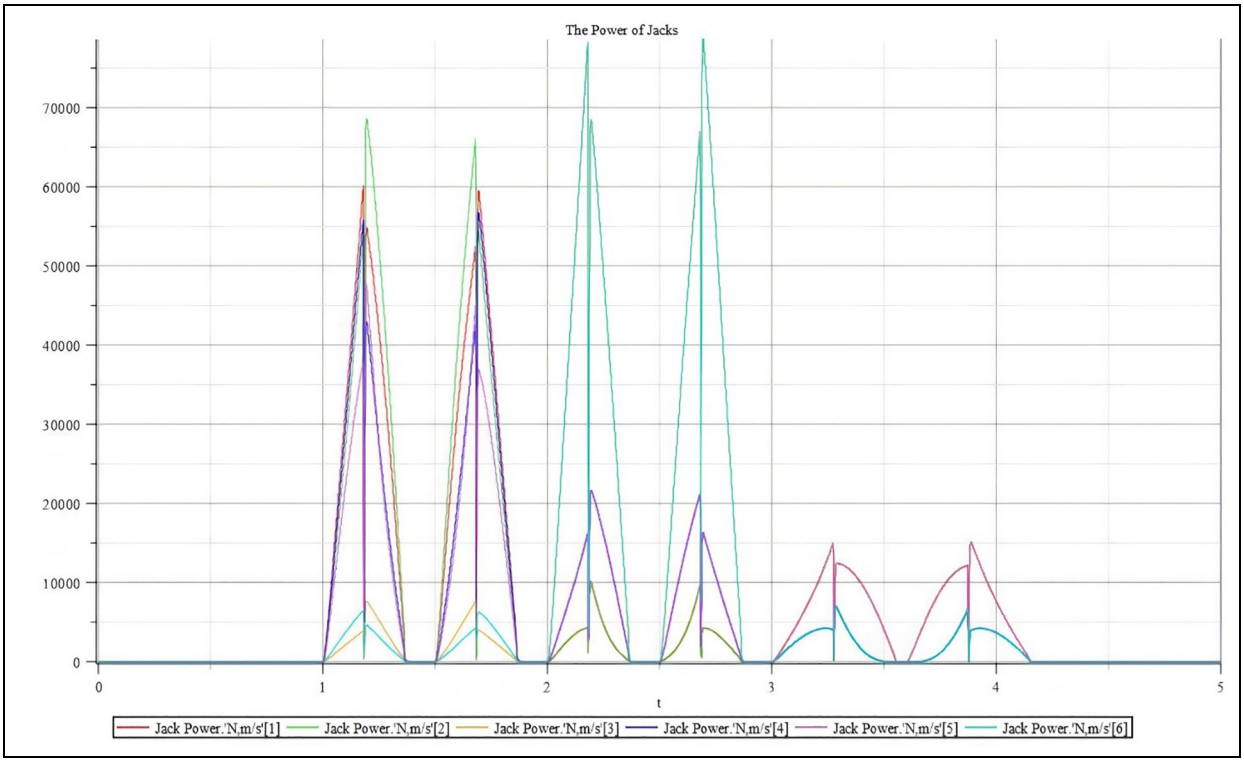

Figure 22. Graph of optimized jacks power (W) in the time domain.

Table 7. Maximum output performance for optimized Stewart platform electric jacks.

Design parameter	Value
Maximum actuator power	42 kW
Actuator displacement range	60 cm
Maximum actuator force	21 kN
Maximum actuator speed under loading	200 cm/s

Declaration of conflicting interests

The author(s) declared no potential conflicts of interest with respect to the research, authorship, and/or publication of this article.

Funding

The author(s) received no financial support for the research, authorship, and/or publication of this article.

ORCID iD

Masood Shahbazi https://orcid.org/0009-0000-8436-4992

References

1. Glozman D and Shoham M. Novel 6-DOF parallel manipulator with large workspace. *Robotica* 2009; 27: 891–895.
2. Zhang X, Mu D, Liu Y, et al. Type synthesis and kinematics analysis of a family of three translational and one rotational pick-and-place parallel mechanisms with high rotational capability. *Adv Mech Eng* 2019; 11: 1687814019853076.
3. Pond G and Carretero JA. Quantitative dexterous workspace comparison of parallel manipulators. *Mech Mach Theory* 2007; 42: 1388–1400.
4. Chen J, San H, Wu X, et al. Structural design and characteristic analysis for a 4-degree-of-freedom parallel manipulator. *Adv Mech Eng* 2019; 11: 1687814019850995.
5. He T, Shao J, Zhang Y, et al. Kinematic performance evaluation of 2-degree-of-freedom parallel mechanism applied in multilayer garage. *Adv Mech Eng* 2018; 10: 1687814018791712.
6. Merlet JP. Determination of the orientation workspace of parallel manipulators. *J Intell Robot Syst* 1995; 13: 143–160.
7. Heerah I, Benhabib B, Kang B, et al. Architecture selection and singularity analysis of a three-degree-of-freedom planar parallel manipulator. *J Intell Robot Syst* 2003; 37: 355–374.
8. Li Y and Xu Q. A new approach to the architecture optimization of a general 3-PUU translational parallel manipulator. *J Intell Robot Syst* 2006; 46: 59–72.
9. Bonev I. The true origins of parallel robots. *ParalleMIC*, 2003.
10. Mallaci G and Oddo R; CAE Inc. *Method and apparatus for damping vibrations in a motion simulation platform*. U.S. Patent 7,806,697, 2010.
11. Thöndel E. Electric motion platform for use in simulation technology–design and optimal control of a linear electromechanical actuator. In: *Proceedings of the world congress on engineering and computer science, vol. 2*, San Francisco, CA, USA, 20–22 October 2010.
12. Idan M and Grunwald A. Analytical evaluation of a simple partial gravity balancing method for limited-power flight simulation. In: *Modeling and simulation technologies conference and exhibit*, Portland, OR, USA, 9–11 August 1999, p.4029. Reston, VA: AIAA.
13. Wang J, Wu J, Wang L, et al. Simplified strategy of the dynamic model of a 6-UPS parallel kinematic machine for realtime control. *Mech Mach Theory* 2007; 42: 1119–1140.
14. Pedrammehr S, Mahboubkhah M and Khani N. Improved dynamic equations for the generally configured Stewart platform manipulator. *J Mech Sci Technol* 2012; 26: 711–721.
15. Ting Y, Chen YS and Jar HC. Modeling and control for a Gough-Stewart platform CNC machine. *J Robot Syst* 2004; 21: 609–623.
16. Guo H and Li H. Dynamic analysis and simulation of a six degree of freedom Stewart platform manipulator. *Proc IMechE, Part C: J Mechanical Engineering Science* 2006; 220: 61–72.
17. Tsai MS and Yuan WH. Dynamic modeling and decentralized control of a 3 PRS parallel mechanism based on constrained robotic analysis. *J Intell Robot Syst* 2011; 63: 525–545.
18. Kazezkhan G, Xiang B, Wang N, et al. Dynamic modeling of the Stewart platform for the NanShan Radio Telescope. *Adv Mech Eng* 2020; 12: 1687814020940072.
19. Tsai LW. Solving the inverse dynamics of a Stewart-Gough manipulator by the principle of virtual work. *J Mech Des* 2000; 122: 3–9.
20. Kalani H, Rezaei A and Akbarzadeh A. Improved general solution for the dynamic modeling of Gough–Stewart platform based on principle of virtual work. *Nonlinear Dyn* 2016; 83: 2393–2418.
21. Asadi F and Sadati SH. Full dynamic modeling of the general Stewart platform manipulator via Kane's method. *Iran J Sci Technol Trans Mech Eng* 2018; 42: 161–168.
22. Kelaiaia R and Zaatri A; Olivier Company. Multiobjective optimization of 6-dof UPS parallel manipulators. *Adv Robot* 2012; 26: 1885–1913.
23. Liu Z, Tang X, Shao Z, et al. Dimensional optimization of the Stewart platform based on inertia decoupling characteristic. *Robotica* 2016; 34: 1151–1167.
24. Shariatee M and Akbarzadeh A. Optimum dynamic design of a Stewart platform with symmetric weight compensation system. *J Intell Robot Syst* 2021; 103: 66.
25. Zhang S, Yuan X, Docherty PD, et al. An improved particle swarm optimization algorithm and its application in solving forward kinematics of a 3-DoF parallel manipulator. *Proc IMechE, Part C: J Mechanical Engineering Science* 2021; 235: 896–907.

26. Yin Z, Qin R and Liu Y. A new solving method based on simulated annealing particle swarm optimization for the forward kinematic problem of the Stewart–Gough platform. *Appl Sci* 2022; 12: 7657.
27. Shirazi AR, Fakhrabadi MMS and Ghanbari A. Optimal design of a 6-DOF parallel manipulator using particle swarm optimization. *Adv Robot* 2012; 26: 1419–1441.
28. Kucuk S. Energy minimization for 3-RRR fully planar parallel manipulator using particle swarm optimization. *Mech Mach Theory* 2013; 62: 129–149.
29. Li L, Zhu Q and Xu L. Solution for forward kinematics of 6-dof parallel robot based on particle swarm optimization. In: *2007 international conference on mechatronics and automation*, Harbin, China, 5–8 August 2007, pp.2968–2973. New York: IEEE.
30. Aldeen Joumah A and Albitar C. Design optimization of 6-RUS parallel manipulator using hybrid algorithm. *Int J Inf Technol Comput Sci* 2018; 10: 83–95.
31. Farooq SS, Baqai A and Butt SU. Multi objective optimization of a Tricept parallel manipulator using evolutionary algorithm. In: *25th international conference on flexible automation and intelligent manufacturing*, FAIM, vol. 1, pp.624–631, 2015.
32. Kumar R, Kumar K, Enferadi J, et al. An optimized approach of intelligent path planning of a robot manipulator using PSO algorithm. *AIP Conf Proc* 2023; 2548: 030024.
33. Nabavi SN, Akbarzadeh A and Enferadi J. Closed-form dynamic formulation of a general 6-P US robot. *J Intell Robot Syst* 2019; 96: 317–330.
34. Nabavi SN, Shariatee M, Enferadi J, et al. Parametric design and multi-objective optimization of a general 6-PUS parallel manipulator. *Mech Mach Theory* 2020; 152: 103913.